Journal of Molecular Liquids 389 (2023) 122949

Contents lists available at ScienceDirect

Journal of Molecular Liquids

journal homepage: www.elsevier.com/locate/molliq

Low-rank coals as precursors of effective carbonaceous adsorbents for the removal of Rhodamine B

Aleksandra Bazan-Wozniak [a,*], Agnieszka Nosal-Wiercińska [b], Selehattin Yilmaz [c], Robert Pietrzak [a]

[a] Adam Mickiewicz University in Poznań, Faculty of Chemistry, Department of Applied Chemistry, Uniwersytetu Poznańskiego 8, 61-614 Poznań, Poland
[b] Maria Curie-Sklodowska University in Lublin, Faculty of Chemistry, Institute of Chemical Sciences, Department of Analytical Chemistry, Maria Curie-Sklodowska 3, 20-031 Lublin, Poland
[c] Canakkale Onsekiz Mart University, Faculty of Science, Department of Chemistry-Analytical Chemistry, 17100 Canakkale, Turkey

ARTICLE INFO

Keywords:
Activated carbon
Chemical activation
wastewater treatment Rhodamine B
Adsorption
Mechanism
Desorption

ABSTRACT

This article presents the potential of two activated carbons obtained through the chemical activation of low-rank coals from the collieries Labin and Spitsbergen using potassium hydroxide for the adsorption of Rhodamine B dye. The results showed that the obtained adsorbents exhibit a mesoporous texture, and the acidic-basic character of the synthesized adsorbents depends on the starting material. The pseudo-second order kinetic model provided the best fit to the experimental results, indicating that the adsorption process occurred following a chemical process. On the other hand, the Langmuir adsorption isotherm showed the best fit, indicating monolayer adsorption. The Langmuir adsorption isotherm exhibited a high maximum adsorption capacity, which was 175 mg/g and 82 mg/g. Negative values of the Gibbs free energy indicating that the removal of Rhodamine B could be thermodynamically favorable due to the spontaneous nature of the adsorption. The efficiency of Rhodamine B removal by the obtained activated carbons depends on the functional groups present on the surface of the synthesized adsorbents, as well as their porous structure. In turn, desorption studies showed that the most effective eluent was the 0.1 M hydrochloric acid solution.

1. Introduction

Global economic growth and ongoing urbanization have led to wastewater from industries such as textiles, metallurgy, and mining containing high levels of toxic organic and inorganic pollutants [1]. These pollutants include dyes, pesticides, metal ions, pharmaceuticals, as well as contaminants from households [2]. While these compounds can cause various side effects ranging from mild to chronic, they affect not only humans but also animals and plants [3]. Water pollution has become a global problem as it has harmful effects on ecosystems, thus contributing to climate change. Scientific research leaves no doubt that climate change is advancing and increasingly impacting our lives [4].

In the past few decades, the world has been primarily concerned with combating organic dyes as the main pollutants. These types of compounds can be divided into two basic categories: ionic and non-ionic dyes. Within the group of ionic dyes, cationic and anionic compounds are distinguished based on the functional groups present in the dye's structure [5,6]. Scientists pay much more attention to ionic dyes as they can pose a significantly greater threat due to their higher reactivity and potential carcinogenic properties compared to other organic compounds [7]. Previous efforts to remove organic dyes from industrial wastewater have focused on adsorption methods. The adsorption process is considered effective, cost-efficient, and environmentally friendly [8]. Several mechanisms, such as electrostatic interactions, hydrogen bonding, π-π interactions, and ion exchange, contribute to the interactions between the dye and the adsorbent during the adsorption process [9,10]. Understanding the adsorption mechanism is crucial, and this process depends not only on the operating conditions (temperature, and pH concentrations) but also on the chemical structure of the targeted compounds [11].

A significant number of organic dyes are released into the natural environment during dyeing processes in industries such as textiles and dyeing. One of these dyes is Rhodamine. This compound is difficult to biodegrade, and its potential toxicity and harmfulness to the natural environment have prompted extensive research on this substance. It is also worth noting that even low-level (low concentration) consumption

* Corresponding author.
E-mail address: aleksandra.bazan@amu.edu.pl (A. Bazan-Wozniak).

https://doi.org/10.1016/j.molliq.2023.122949
Received 15 July 2023; Received in revised form 22 August 2023; Accepted 28 August 2023
Available online 28 August 2023

of Rhodamine by aquatic animals can cause damage to the respiratory and reproductive systems, and even cancer [12,13].

Activated carbons are among the most effective and promising carbon-based adsorbents used for wastewater treatment of organic dyes [14]. The adsorbents used in adsorption processes should be environmentally friendly, efficient, and derived from as few reagents as possible. Undoubtedly, activated carbons meet these requirements [15].

The article presents the synthesis of adsorbents from low-rank coals from the collieries Labin and Spitsbergen. The prepared activated carbons were examined using various techniques to determine the surface morphology, structure, elemental composition, porosity, and acid-base properties of all the activated carbons that were prepared. The kinetics and adsorption mechanism of Rhodamine B from an aqueous solution were investigated. The impact of reaction parameters such as temperature and pH changes, reaction time, dye concentration, adsorbent mass, and sample shaking rate on the efficiency of dye removal by the obtained adsorbents, was assessed.

2. Materials and methods

2.1. Preparation of precursors

In this study, low-rank coals were used as precursors: coals from the collieries Labin and Spitsbergen. The raw materials were sieved through a 0.09 mm mesh size and subjected to demineralization. 250 g of each precursor was treated with 200 mL of concentrated hydrochloric acid and left for 24 h. After this time, the coals were thoroughly washed with hot distilled water (10 L) until they reached a neutral pH. The washed precursors were then treated with 200 mL of 40 % hydrofluoric acid and also left for 24 h. Afterward, the samples were rinsed with hot distilled water (10 L) to remove fluoride ions. The demineralized coals were dried at 110 °C until a constant weight was achieved.

2.2. Preparation of the activated carbons

The activation of the coals was carried out in a tubular furnace (conventional heating). The process was conducted at a temperature of 600 °C, in a nitrogen atmosphere (330 mL/min) for a duration of 45 min. Potassium hydroxide was used as the activating agent, with a weight ratio of 2:1 to the precursor. To remove excess activator, the activated carbons were thoroughly washed with 5 % hydrochloric acid and distilled water at hot temperatures until reaching a neutral pH. The adsorbents were then dried at 110 °C.

2.3. Physical and chemical characterization

The elemental composition of the samples was analyzed using the Vario EL III elemental analyzer (Elementar Analysensysteme GmbH, Germany). The total ash content was determined by burning the samples in a microwave muffle furnace (Phoenix, CEM Corporation, USA). The morphology of the activated carbons was characterized using scanning electron microscopy (PHILIPS, Netherlands). The surface area and nitrogen adsorption/desorption isotherm were analyzed using a surface area and porosity analyzer Autosorb iQ (Quantachrome, USA). The content of surface oxygen functional groups, including acidic and basic groups, was determined using the Boehm method [16].

2.4. Determination of pH_{pzc} of the activated carbons

For each of the activated carbons, the point of zero charge (pH_{pzc}) was determined. To achieve this, six beakers were filled with 100 mL of 0.1 M NaCl solution, and the pH was adjusted from 2 to 12 using 0.1 M NaOH/HCl solutions. Nitrogen gas was then bubbled through the solution to stabilize it and remove CO_2. Next, a solution of NaCl (50 mL) was mixed with 0.2 g of the activated carbon samples and stirred for 24 h. Afterward, the final pH (pH_{final}) was measured. The initial pH ($pH_{initial}$) was plotted against pH_{final} to determine the pH_{pzc}.

2.5. Adsorption of Rhodamine B

The adsorption processes were carried out by using a UV–VIS spectrophotometer at a wavelength of 554 nm. In the initial stage, the effect of the adsorbent mass on the efficiency of dye removal was determined. Three masses of activated carbon were used: 10, 20, and 30 mg. The experiments were conducted on a laboratory shaker (Heidolph) at a shaking speed of 300 rpm. The samples were placed in 100 mL Erlenmeyer flasks and mixed with 50 mL of a 30 mg/L solution of Rhodamine B. The mixtures were shaken for 8 h, and after that, the solid samples were separated from the solution using a laboratory centrifuge. The subsequent step involved conducting spectrophotometric analysis. The amount of adsorbed Rhodamine B (1) and the percentage of dye removal (2) were determined using the following formulas:

$$q_e = \frac{(C_0 - C_e) \times V}{m} \tag{1}$$

$$Removal(\%) = \frac{(C_0 - C_e)}{m} \times 100\% \tag{2}$$

where C_0 and C_e are the initial and equilibrium concentrations of Rhodamine B (mg/L), V is the volume of the solution (L), m is the mass of $Labin_{KOH}$/$Spitsbergen_{KOH}$ (g), and q_e is the amount of adsorbed Rhodamine B (mg/g).

The effect of shaking speed on the activated carbons was studied at three values: 200, 300, and 400 rpm (mass of activated carbon: 20 mg, volume of dye solution: 50 mL, dye concentration: 30 mg/L, process duration: 8 h).

Subsequent adsorption tests were conducted using a mass of 20 mg of activated carbon, a shaking speed of 300 rpm, and a volume of 50 mL of dye solution. The adsorption processes were carried out for 8 h. The influence of the initial concentration of Rhodamine B solution on the sorption capacities of the tested adsorbents was determined within the concentration range of 10–80 mg/L.

The study employed the following adsorption isotherm models: Langmuir, Freundlich, Temkin, and Dubinin-Radushkevich models [17]. The Langmuir isotherm model (3) assumes monolayer adsorption theory:

$$\frac{C_e}{q_e} = \frac{1}{K_L \times q_{max}} + \frac{C_e}{q_{max}} \tag{3}$$

where the parameters K_L (Langmuir constant, L/mg) and q_{max} (maximum adsorption capacity, mg/g) can be determined based on the intersection and slope of the plot of C_e/q_e versus C_e. The shape of the Langmuir isotherm can be expressed using the dimensionless separation factor R_L (4), defined as:

$$R_L = \frac{1}{1 + K_L \times C_0} \tag{4}$$

The value of R_L reflects the shape and nature of the isotherm. When the coefficient takes a value of $0 < R_L < 1$, it indicates a favorable adsorption process. When $R_L = 1$, the isotherm is linear. On the other hand, when $R_L = 0$, the process is irreversible.

The Freundlich isotherm model (5) is used to describe the adsorption process occurring on adsorbents with a heterogeneous structure:

$$lnq_e = lnK_F + \frac{1}{n} lnC_e \tag{5}$$

where K_F $(mg/g(L/mg)^{1/n})$ is the Freundlich constant and 1/n is a constant related to the intensity of the adsorption process.

In the Temkin isotherm model, the equation (6) is represented as:

$$lnq_e = BlnA_T + BlnC_e \tag{6}$$

where B (J/mol) and A_T (L/mg) are Temkin constants that can be calculated from the q_e versus $\ln(C_e)$ plot. The Temkin isotherm equation assumes that the heat of adsorption for all molecules in the layer decreases linearly due to the adsorbent-adsorbate interactions, and the adsorption is characterized by a uniform distribution of binding energies.

The last model of adsorption isotherm used in this study is the Dubinin-Radushkevich model, which is based on the mechanism of pore filling and assumes a heterogeneous surface with a variable adsorption potential. It is represented by the equation (7):

$$lnq_e = lnq_m - \beta\varepsilon^2 \tag{7}$$

where ε represents the Polanyi potential, and β (mol^2/kJ^2) is the constant associated with the adsorption energy, enabling the calculation of the free energy - E (kJ/mol) (8):

$$E = \frac{1}{\sqrt{2\beta}} \tag{8}$$

Knowing the kinetic parameters of the adsorption process enables a comprehensive assessment of the adsorptive capacities of the activated carbons used. The most commonly used kinetic models for adsorption include the pseudo-first order (PFO), pseudo-second order (PSO), Elovich, and intraparticle diffusion models [18].

The process described by the pseudo-first order model (9) represents reversible interactions in an equilibrium state between the liquid and solid phases, and is expressed by the equation:

$$\log(q_e - q_t) = logq_e - \frac{k_1 t}{2.303} \tag{9}$$

where q_t (mg/g) represents the amount of adsorbed pollutant at a given time t (min), and k_1 (1/min) is the rate constant of the pseudo-first order adsorption process.

On the other hand, the pseudo-second order model (10) assumes that the rate-controlling step of the adsorption process most likely involves chemical interactions leading to the binding of organic compounds on the surface of the adsorbent based on an ion exchange mechanism:

$$\frac{t}{q_t} = \frac{1}{k_2 q_e^2} + \frac{t}{q_e} \tag{10}$$

where k_2 (g/mg × min) is the rate constant of the pseudo-second order adsorption model.

The general form of the Elovich model (11) is as follows:

$$q_t = \frac{1}{\beta}\ln(\alpha\beta) + \frac{1}{\beta} lnt \tag{11}$$

where α represents the initial adsorption rate (mg/g × min) and β is the desorption constant (g/mg).

The last kinetic model utilized in this study was the intraparticle diffusion model (12):

$$q_t = k_{IPD} t^{1/2} + C \tag{12}$$

where k_{IPD} is the intraparticle diffusion rate constant (mg/g × $min^{1/2}$) and C is a constant (mg/g) providing information about the thickness of the boundary layer.

During further investigations, the effect of temperature on the efficiency of dye removal was examined. The experiments were conducted at various temperature conditions. The results enabled the determination of thermodynamic parameters [19] such as the standard change in free energy ΔG^0 (kJ/mol), enthalpy ΔH^0 (kJ/mol), and entropy ΔS^0 (J/mol × K). The following equations (13–16) were used:

$$\Delta G^0 = -RTlnK_d \tag{13}$$

$$\Delta G^0 = \Delta H^0 - T\Delta S^0 \tag{14}$$

$$K_d = q_e/C_e \tag{15}$$

$$lnK_d = \frac{\Delta S^0}{R} + \frac{\Delta H^0}{RT} \tag{16}$$

where K_d (L/g) is the distribution coefficient for the adsorption, T (K) is the absolute temperature and R is the gas constant 8.314 (J/mol × K).

After the adsorption experiments, the Rhodamine B-laden $Labin_{KOH}$/$Spitsbergen_{KOH}$ samples were separated by filtration. The samples were gently washed with double-distilled water to remove any unadsorbed Rhodamine B. The activated carbons were then agitated with solutions of NaOH (0.1 M), HCl (0.1 M), or H_2O. The desorbed Rhodamine B in the solution was separated by centrifugation and analyzed as described previously.

3. Results and discussion

3.1. Characterization of the precursors and activated carbons

The elemental analysis ~~is~~ presented in Table 1. It can be observed that the precursors used in the study exhibit a diverse elemental carbon content. The Labin coal exhibits nearly twice as much C^{daf} as the Spitsbergen coal. The lower content of this element in the Spitsbergen sample is attributed to the significant presence of ash in the coal's structure. The mineral matter in this material constitutes as much as 48.9 wt. %. As expected, the Labin sample recorded a high S^{daf} content of 11.4 wt. %. It was observed that the demineralization of Labin coal led to an increase in carbon, hydrogen, and nitrogen content, as well as a decrease in the remaining two analyzed elements. Washing Labin coal with hydrochloric and hydrofluoric acid solutions resulted in a reduction in O^{daf} content due to the removal of oxygenated functional groups. This, in turn, led to an increase in C^{daf} content in the $Labin_{demineralized}$ sample. Slightly different changes were observed in the case of the second starting material (a decrease in hydrogen and nitrogen content compared to the precursor). As anticipated, the demineralization of the starting materials contributed to a reduction in the mineral matter content in the produced materials.

The results obtained from the elemental analysis also demonstrate that the activation of demineralized precursors using KOH leads to a percentage increase in elemental carbon content in the structure of the produced activated carbons. The percentage value of C^{daf} presented in Table 1 indicates that while the $Labin_{KOH}$ activated carbon exhibits the highest content of this element in its structure (77.7 wt. %), the largest increase in C^{daf} (compared to the precursor) was observed in the case of $Spitsbergen_{KOH}$. Both activated carbons also exhibited a lower content of the four remaining elements compared to the starting materials. The lower hydrogen content in the activated carbons relative to the precursors is a consequence of the gasification of hydrogen-rich fragments of the precursor. Conversely, the decrease in nitrogen and sulfur content in the obtained adsorbents likely indicates a low resistance of nitrogen/sulfur groups to the action of the activating agent during the activation process. Furthermore, the chemical activation process contributes to a decrease in ash content in the $Labin_{KOH}$ and $Spitsbergen_{KOH}$ samples.

Fig. 1 depicts the nitrogen adsorption/desorption isotherms for the $Labin_{KOH}$ and $Spitsbergen_{KOH}$ samples. The shape of the curves indicates

Table 1
Characteristic of the studied coals (elemental analysis's), (wt. %).

Coal	C^{daf}	H^{daf}	N^{daf}	S^{daf}	O^{daf*}	Ash
Labin	68.3	5.0	1.2	11.4	14.1	14.1
$Labin_{demineralized}$	75.7	5.2	2.4	10.6	9.7	7.3
$Labin_{KOH}$	77.7	1.4	1.1	3.9	15.9	6.5
Spitsbergen	37.4	3.0	0.3	0.6	58.7	48.9
$Spitsbergen_{demineralized}$	44.4	1.1	0.4	0.5	53.6	36.6
$Spitsbergen_{KOH}$	62.6	0.9	0.2	0.4	35.9	27.7

dry – dry ash-free basis, * - by difference.

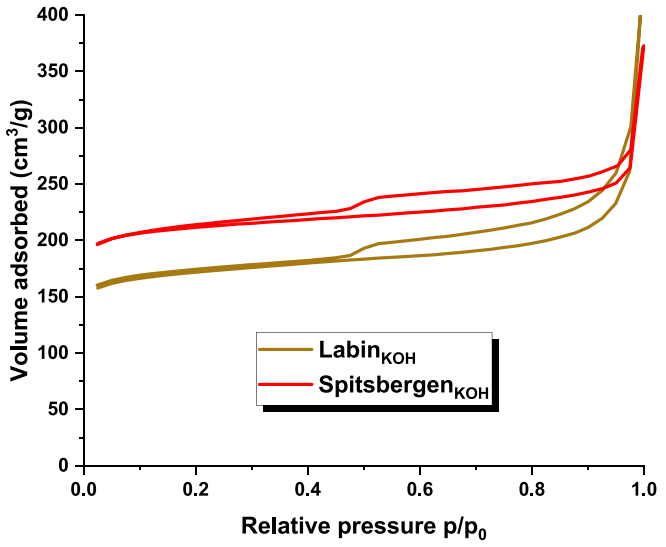

Fig. 1. Low-temperature N_2 adsorption–desorption isotherms of $Labin_{KOH}$ and $Spitsbergen_{KOH}$.

that they exhibit Type IV isotherms according to the IUPAC classification, characterized by a distinct hysteresis loop. This suggests that the obtained carbon adsorbents contain mesopores their structure.

SEM images presented in Fig. 2. It can be observed that the morphological structure of $Labin_{KOH}$ carbon is irregular and contains numerous pores, suggesting that adsorbed molecules will readily penetrate the surface of this carbon. On the other hand, the morphological structure of the activated carbon obtained from Spitsbergen coal resembled a flat rock without visible pores. Additionally, brighter areas (aggregates) were observed on the surface of $Spitsbergen_{KOH}$, indicating the presence of mineral matter on its surface. The textural parameters of the activated carbons presented in Table 2. It was found that the $Labin_{KOH}$ sample has a surface area of 623 m^2/g, while the $Spitsbergen_{KOH}$ coal has a surface area of 510 m^2/g. The obtained surface areas are lower compared to the activated carbons obtained from the activation of lignite coal and pine sawdust using potassium hydroxide [20]. This could be attributed to the fact that the used precursors, especially Spitsbergen coal, contained significant amounts of mineral matter in their structure. These minerals might have blocked or clogged the pores, thereby preventing effective reaction between the precursor and the activating agent (potassium hydroxide) from occurring. The activated carbons obtained in this article exhibited comparable or even better textural parameters compared to mesoporous activated carbons obtained from lignite coal [21]. Further analysis of the data presented in Table 2 confirms that the obtained adsorbents are predominantly composed by mesopores. According to the classification proposed by the International Union of Pure and Applied Chemistry, pores are divided into three main groups: micropores (pore diameter < 2 nm), mesopores (2 nm $<$ pore diameter < 50 nm), and macropores (pore diameter > 50 nm) [22]. The significant presence of mesopores in the structure of the synthesized adsorbents was further confirmed in Fig. 3, which depicts the pore size distribution in the $Labin_{KOH}$ and $Spitsbergen_{KOH}$ samples. Furthermore, considering the values of total pore volume and micropore volume, it can be concluded that the $Labin_{KOH}$ coal contains more micropores in its structure.

Understanding the acid-base properties of the adsorbents used in carbon material studies is crucial because it enables us to predict which pollutants a specific activated carbon will effectively adsorb. Oxygen functional groups play a significant role in this aspect, as they can exhibit either acidic or basic characteristics. In the research on carbon adsorbents, various surface modification processes are employed to introduce specific functional groups. However, each of these processes incurs additional costs. Therefore, it is beneficial for the produced activated carbon to have numerous functional groups in its structure without the need for additional surface modification. By employing the Boehm titration method, the quantitative amounts of surface functional groups were determined for all the carbon materials presented in this study (Fig. 4). Labin coal is characterized by a significant excess of basic groups over acidic groups (basic groups: 2.51 mmol/g, acidic groups: 0.21 mmol/g), whereas the second precursor exhibits comparable acid-base properties with a slight excess of acidic groups (0.61 mmol/g) over basic groups (0.49 mmol/g). The demineralization process for both precursors resulted in a decrease in basic groups and the formation of new acidic functional groups. It was observed that oxygen functional groups are more abundant in the demineralized Labin sample. The use of potassium hydroxide as an activating agent further influenced the acid-base properties of the obtained samples, which were dependent on the precursor. $Labin_{KOH}$ exclusively possesses acidic groups on its surface (1.50 mmol/g), while for $Spitsbergen_{KOH}$ coal, the completely opposite trend was observed (sole presence of basic groups – 2.44 mmol/g). The dominant basicity of the $Spitsbergen_{KOH}$ sample can be attributed to the presence of chromene and pyrone-like groups, as well as a significant amount of mineral matter that resides in the pores of the produced adsorbent. Conversely, the acidic character of the $Labin_{KOH}$ sample may be attributed to the presence of a substantial amount of sulfur-containing groups.

The pH_{pzc} (point of zero charge) values of $Labin_{KOH}$ and $Spitsbergen_{KOH}$ were determined using the drift method (Fig. 5). The pHpzc for $Labin_{KOH}$ is 7.9, while for $Spitsbergen_{KOH}$, it is 6.3. According to the definition of the point of zero charge, the surface of activated carbons is negatively charged when $pH > pH_{pzc}$ and positively charged below this value. In the adsorption studies, the cationic dye Rhodamine B was used, suggesting that the effective removal of the dye by the obtained activated carbons should occur effectively at pH values of the adsorbate higher than the pH_{pzc} values of the samples. This is due to the stronger electrostatic attraction between the cationic dye and the negatively

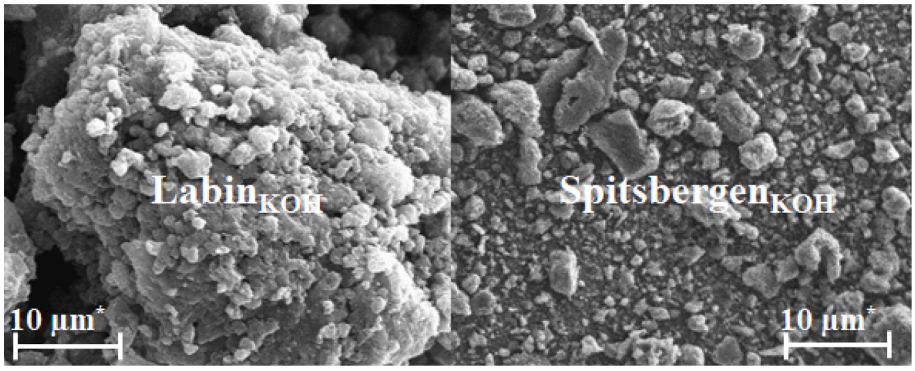

Fig. 2. SEM photographs of $Labin_{KOH}$ and $Spitsbergen_{KOH}$.

Table 2
Textural parameters of $Labin_{KOH}$ and $Spitsbergen_{KOH}$.

Sample	Surface area (m^2/g)	Micropore area (m^2/g)	Total pore volume (cm^3/g)	Micropore volume (cm^3/g)	Average pore diameter (nm)
$Labin_{KOH}$	623	562	0.58	0.31	3.71
$Spitsbergen_{KOH}$	510	450	0.62	0.25	4.89

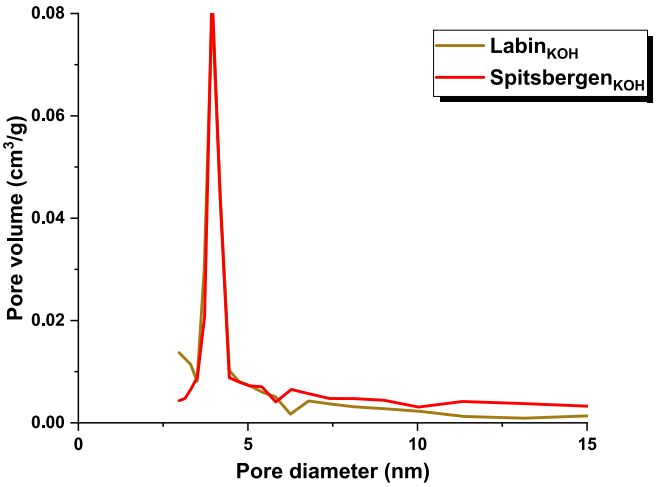

Fig. 3. Pore size distributions of $Labin_{KOH}$ and $Spitsbergen_{KOH}$.

charged surface of the activated carbons [23].

3.2. Adsorption study

The adsorption studies started with determining how the mass of the adsorbent affects the efficiency of dye removal. The results of the studies are presented in Fig. 6a and 6b. It was observed that with an increase in the mass of $Labin_{KOH}$ and $Spitsbergen_{KOH}$ samples, the sorption capacity towards the aqueous solution of Rhodamine B decreases (Fig. 6a), while the percentage of dye removal increases (Fig. 6b). The decrease in sorption capacity was greater for $Labin_{KOH}$. The reduction of adsorption capacity with an increase of the adsorbent mass of activated carbons can be attributed to factors such as the concentration of Rhodamine B, volume, and saturation of adsorption sites due to the interaction of particles, such as accumulation across the entire surface, and an increase in the diffusion path length. The increase in the mass of the adsorbent also resulted in an increase in the effectiveness of the process. Increasing the mass of the carbon led to an increased contact surface area and, therefore, an increased number of active sites capable of adsorbing the dye [24]. For the $Labin_{KOH}$ sample, the percentage adsorbed increased from 96.67 % for a mass of 10 mg of carbon to 97. 90 % for a mass of 20 mg and 99. 35 % for a mass of 30 mg. For the second activated carbon, the percentage adsorbed increased from 71.43 % for a mass of 10 mg of carbon to 85. 56 % for a mass of 20 mg and 87.01 % for a mass of 30 mg. Regardless of the activated carbon used, increasing the mass of the adsorbent from 20 mg to 30 mg resulted in only an approximately 2 % increase in dye removal efficiency. This may due to the overlapping of the adsorption sites as a result of overcrowding of adsorbent particles.

The next parameter that can be helpful in interpreting the obtained dependencies is the shaking speed of the samples. The impact of this parameter was investigated in the range of 200 to 400 rpm for an adsorbent mass of 20 mg, a dye volume of 50 mL, and a Rhodamine B concentration of 30 mg/L at a temperature of 22 °C ± 1. The results of sorption capacities obtained at different shaking speeds for $Labin_{KOH}$ and $Spitsbergen_{KOH}$ carbons were presented in Fig. 6c. As shown in Fig. 6c, both adsorbents displayed a consistent trend. The sorption capacity for the aqueous Rhodamine B solution increased as the shaking speed was raised from 200 to 300 rpm. Subsequently, the capacity stayed relatively stable as the shaking speed was raised further to 400 rpm. These results imply an optimal shaking speed within the range of 200–300 rpm which the sorption capacity remains essentially constant. The above effect may be ascribed to the decrease in the thickness of the boundary layer around the carbons particles because of an increase in the degree of mixing. When the mixture was shaken, the activated carbons particles move rapidly in the solution, which increases the concentration of Rhodamine B near the surface of the adsorbents, possibly reaching levels near the total concentration. Nevertheless, as the shaking speed exceeded 400 rpm, diffusion rates started to decrease. This may occur because the high shaking speed provided sufficient additional energy to break newly formed bonds between the Rhodamine B and the activated carbon surface [24]. Therefore, further adsorption studies were conducted at a shaking speed of 300 rpm and a coal mass of 20 mg.

In the subsequent stages of the conducted research, the adsorption capacity of the activated carbons towards the specific organic pollutant was determined. The experimental adsorption capacities of the employed adsorbents were found to be: 174 mg/g for $Labin_{KOH}$ coal and

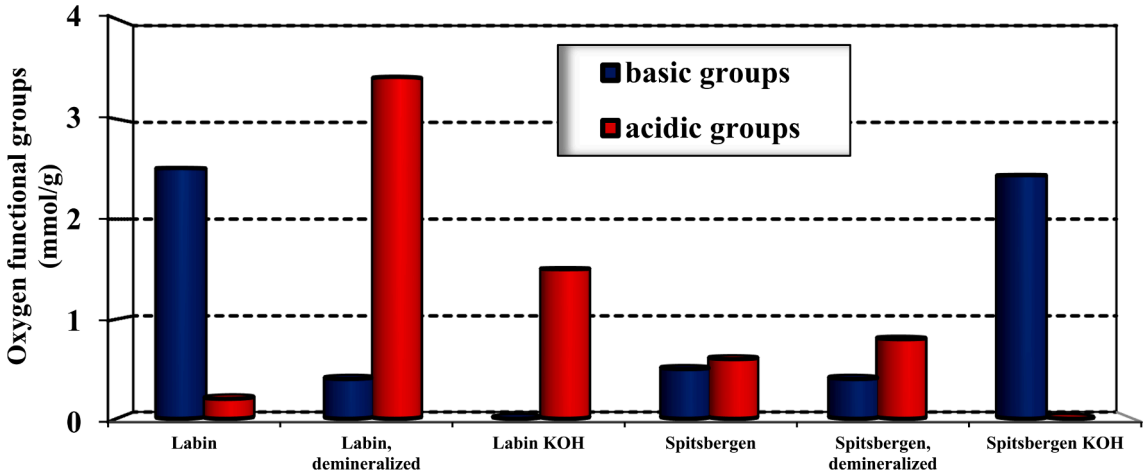

Fig. 4. Acid-base properties of $Labin_{KOH}$ and $Spitsbergen_{KOH}$.

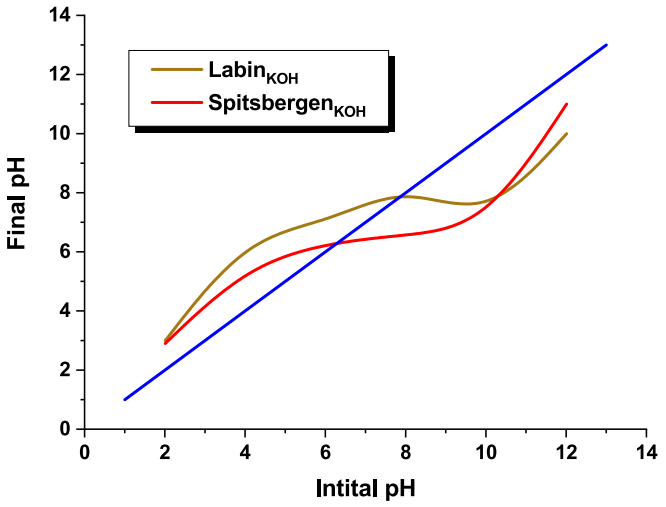

Fig. 5. Point of zero charge of Labin$_{KOH}$ and Spitsbergen$_{KOH}$.

80 mg/g for the Spitsbergen$_{KOH}$ sample (Table 3). Although the same activation procedure was applied to both precursor materials, the obtained adsorption capacities exhibit significant disparities. Several factors might contribute to these variations in the outcomes. The fact that the adsorption of organic compounds is a complex and intricate process is widely acknowledged. Therefore, determining the above parameters is of utmost importance. Based on the data presented in Table 2, it is apparent that the specific surface area (S_{BET}) and the degree of developed porous structure of the obtained adsorbents might exert an influence on the adsorption capacities. The Labin$_{KOH}$ sample displayed a higher S_{BET} value, resulting in a greater adsorption capacity compared to the Spitsbergen$_{KOH}$ adsorbent. However, this parameter might not have a decisive impact, considering the difference in specific surface area between Labin$_{KOH}$ and Spitsbergen$_{KOH}$ is only slightly above 100 m^2/g. The chemical nature of the activated carbons might indeed play a major role in this context. Labin$_{KOH}$ exhibited a pronounced acidic surface character, whereas the other examined adsorbent displayed a basic nature. In aqueous systems acidic functional groups undergo dissociation, leading to a negatively charged surface of the adsorbent. This is particularly relevant in the case of adsorbing cationic dyes such as Rhodamine B. Therefore, the adsorption capacity of Labin$_{KOH}$ was over twice as high as the outcome observed for SpitsbergenK$_{OH}$.

An essential component of the adsorption process involving the aqueous solution of Rhodamine B and the investigated adsorbents is the fitting of acquired experimental data to the relevant adsorption isotherm models. The analysis of the obtained isotherms offers valuable insights into the mechanism, character, and type of interactions between the adsorbate and adsorbent. Four isotherm models were used to determine the equilibrium parameters: Langmuir, Freundlich, Temkin, and Dubinin-Radushkevich. After analyzing the obtained parameters, it was determined that regardless of the activated carbons used, the experimental data fitting aligns most closely with the Langmuir model (Table 3). For this model, the highest correlation coefficient values of R^2 were obtained, measuring 0.995 for the Labin$_{KOH}$ sample and 0.990 for the Spitsbergen$_{KOH}$ sample. The Langmuir isotherm model assumes monolayer adsorption theory [25]. It's worth emphasizing that the sorption capacity coefficient (q_m) closely approximated the experimental values of q_e. Another parameter determined for the Langmuir model was the dimensionless separation factor, and its values indicate a favorable adsorption process of Rhodamine B on the synthesized adsorbents. The final parameter established within this model was the equilibrium constant K_L, which signifies the adsorbent's affinity for the removed pollutant. The higher the equilibrium constant K_L, the greater the sorption capacity of the activated carbon for the adsorbate. Among the utilized adsorbents, the Labin$_{KOH}$ sample demonstrated a stronger affinity for Rhodamine B, a fact further supported by its higher sorption capacity compared to other carbons. For the Temkin and Dubinin-Radushkevich models, significantly lower values of the R^2 parameter were obtained compared to the results obtained for the Langmuir and Freundlich isotherms. Therefore, it is presumed that these models do not play a significant role in understanding the interactions between the guest and host. The equilibrium parameters determined for the Freundlich model, particularly the R^2 parameter, could suggest the occurrence of multilayer adsorption during the adsorption process of Rhodamine B on activated carbons. This suggests the complexity of the adsorption process mechanism. Furthermore, for the Labin$_{KOH}$ and Spitsbergen$_{KOH}$ samples, the empirical constant 1/n was found to be 0.110 and 0.222, respectively. This observation suggests that chemical reactions may occur between the Rhodamine B molecules and the surface functional groups of the activated carbons [26].

The determination of the kinetic parameters of the adsorption process allows a thorough evaluation of the sorption capacity of the activated carbons used. Accurately determined adsorption rate parameters can provide valuable information about the mechanism of the process. The results of the kinetic studies were presented in Fig. 7. From Fig. 7, the optimal duration of the adsorption process can be determined. The maximum efficiency of Rhodamine B removal corresponds to the point where adsorption equilibrium is achieved. This is of great significance from a technological perspective when switching from laboratory-scale to industrial-scale operations. Furthermore, through the optimization of processing time, it becomes feasible to ascertain the equilibrium adsorption parameters, which constitute crucial elements for evaluating the sorption capacity of the employed activated carbons. From the curves, it can be observed that the sorption capacity increased rapidly with contact time. Equilibrium was reached after 240 min, and the experimentally determined maximum sorption capacity for Labin$_{KOH}$ was 73 mg/g, while for the Spitsbergen$_{KOH}$ sample it was 60 mg/g. The initial increase in capacity can be attributed to enhanced contact opportunities between the dye molecules and the synthesized adsorbents.

The kinetic studies focused on determining an appropriate model characterizing the adsorption process. The experimental data were best described by the pseudo-second order model, as indicated by the high value of the fitting coefficient R^2, which is 0.999 for both carbons (Table 4). Moreover, the amount of adsorbed Rhodamine B calculated using the PSO model matched the experimental value q_t. The studied systems also conform to the Elovich model, with high values of the coefficient R^2. The Elovich model is typically used for chemisorption systems on heterogeneous surfaces. In addition, if the value of parameter α is higher than β, the adsorption rate is greater than the desorption rate [18]. In our study, higher values of parameter α were indicative of a swift adsorption process of the dye on the surface of activated carbons. Nevertheless, the PFO model and intraparticle diffusion exhibited notably low R^2 values, ranging from 0.591 to 0.711. This implies that these models may not be suitable for characterizing the kinetics of the investigated pollutant's adsorption onto the acquired samples.

Temperature is another parameter that affects the efficiency of the adsorption process for environmentally harmful organic compounds. Changes in temperature, whether increasing or decreasing, result in variations in the amount of Rhodamine B adsorbed. Furthermore, conducting the process at different temperatures allows for the determination of fundamental thermodynamic parameters such as changes in enthalpy, entropy, and free energy. After analyzing the data presented in Fig. 8 and Table 5, it can be concluded that for both samples, enhancing the process temperature increased the efficiency of dye removal. Increasing the temperature of the reaction system results in Rhodamine B molecules being more mobile, which makes their interaction with the activated carbon surface quicker and more efficient. Additionally, they penetrate deeper into the pores of the adsorbent. Furthermore, negative values of the change in free energy were observed throughout the temperature range, confirming the spontaneous nature of the process due to the increased kinetic energy of Rhodamine B molecules [19].

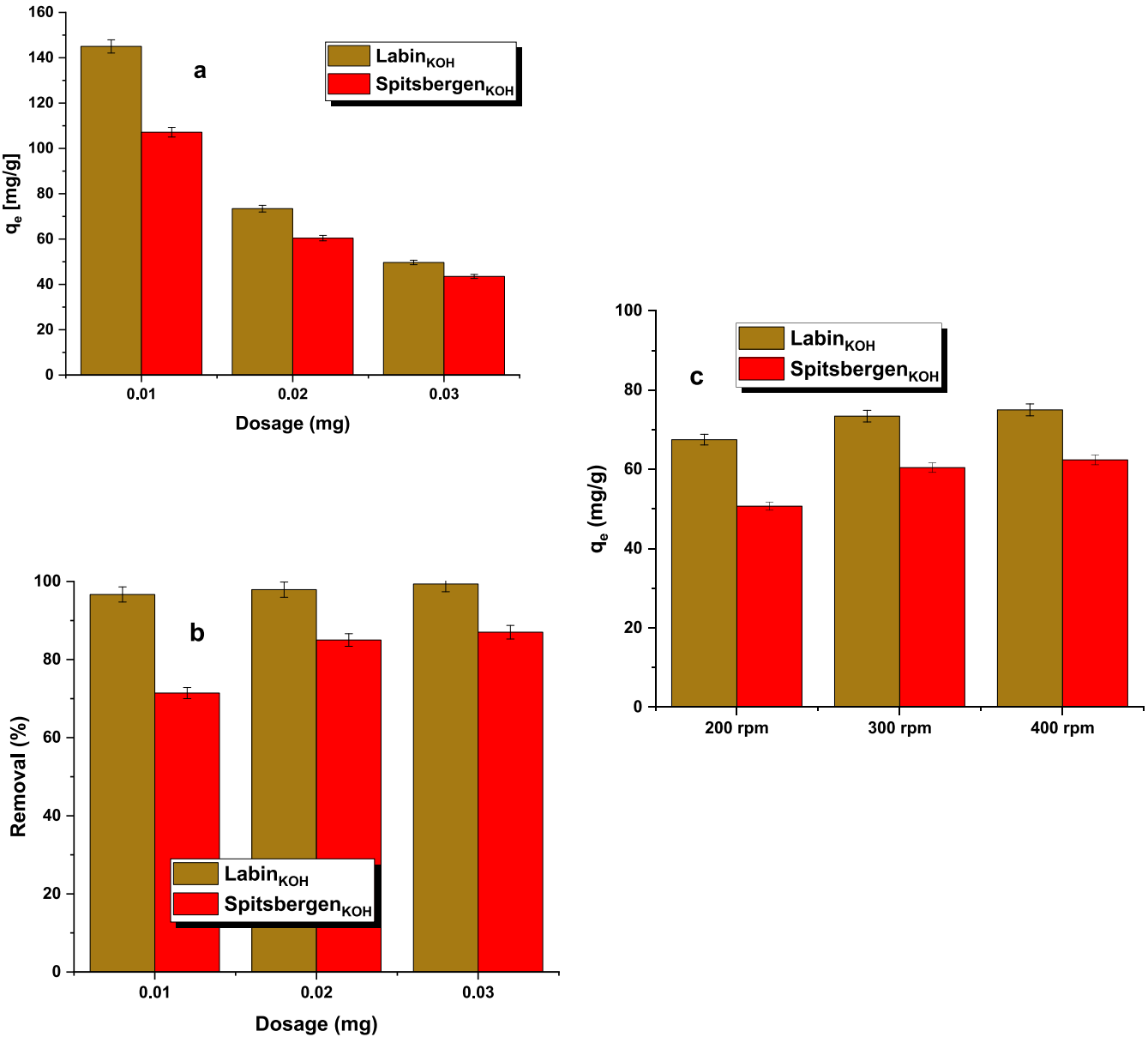

Fig. 6. Impact of changing the Labin$_{KOH}$ and Spitsbergen$_{KOH}$ dose (a,b) and shaking rate (c) samples on Rhodamine B adsorption.

Table 3
Adsorption isotherm parameters of Rhodamine B adsorption on activated carbons.

Isotherms model	Parameters	Activated carbons	
		Labin$_{KOH}$	Spitsbergen$_{KOH}$
	q_e (mg/g)	*174*	*80*
Langmuir	R^2	0.995	0.990
	q_m (mg/g)	175	82
	K_L (L/mg)	0.041	0.029
	R_L	0.235–0.552	0.465–0.776
Freundlich	R^2	0.944	0.942
	K_F (mg/g(L/mg)$^{1/n}$)	138.67	48.42
	1/n	0.110	0.222
Temkin	R^2	0.408	0.649
	B (J/mol)	58.20	103.92
	A_T (L/mg)	10.12	3.65
Dubinin-Radushkevich	R^2	0.839	0.714
	q_m (mg/g)	166	74
	E (kJ/mol)	3.382	1.551

Positive values of the change in enthalpy were obtained using various activated carbons, indicating that the process is endothermic. Additional analysis of the data provided in Table 5 revealed positive changes in entropy too. The calculated ΔS^0 value for the Labin$_{KOH}$ carbon was 195.21 J/mol × K, whereas for the Spitsbergen$_{KOH}$ sample, it was 139.93 J/mol × K. Positive values of this parameter indicate increased randomness at the interface between the activated carbon and the Rhodamine B solution, thereby enhancing the efficiency of dye removal. The higher the value of the ΔS^0 parameter, the more effectively the process occurs [24].

Desorption studies were conducted using three eluents: 0.1 M NaOH/HCl, and distilled water. The results were presented in Fig. 9. The Labin$_{KOH}$ and Spitsbergen$_{KOH}$ carbons were regenerated and reused in adsorption after the dye adsorption process. The process was repeated three times. The best eluent was found to be the hydrochloric acid solution, as acidic conditions cause the displacement of dye molecules from their binding sites by protons. It was observed that the efficiency of Rhodamine B removal decreased after each cycle. Therefore, further modifications are required to improve the suitability of the obtained

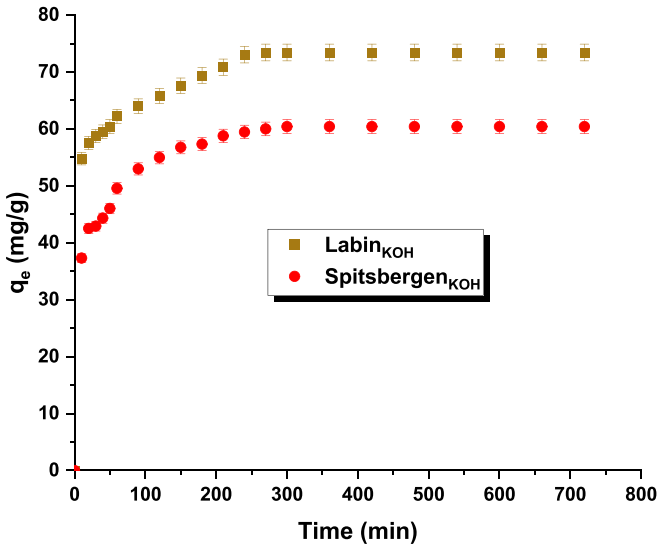

Fig. 7. Adsorption isotherm for Rhodamine B on Labin$_{KOH}$ and Spitsbergen$_{KOH}$.

Table 4
Adsorption kinetics parameters of Rhodamine B by Labin$_{KOH}$ and Spitsbergen$_{KOH}$.

Models	Parameters	Sample	
		Labin$_{KOH}$	Spitsbergen$_{KOH}$
	q_t *(mg/g)*	*73*	*60*
PFO	R^2	0.906	0.881
	k_1 (1/min)	9.67×10^{-3}	1.41×10^{-2}
	$q_{e,cal}$ (mg/g)	20	28
PSO	R^2	0.999	0.999
	k_2 (g/mg × min)	1.94×10^{-3}	1.17×10^{-3}
	$q_{e,cal}$ (mg/g)	74	62
Intraparticle diffusion model	R^2	0.591	0.711
	k_{IPD} (mg/g × $min^{1/2}$)	3.034	2.663
	C (mg/g)	33	23
Elovich	R^2	0.952	0.980
	α (mg/g × min)	41.59	101.28
	β (g/mg)	0.094	0.137

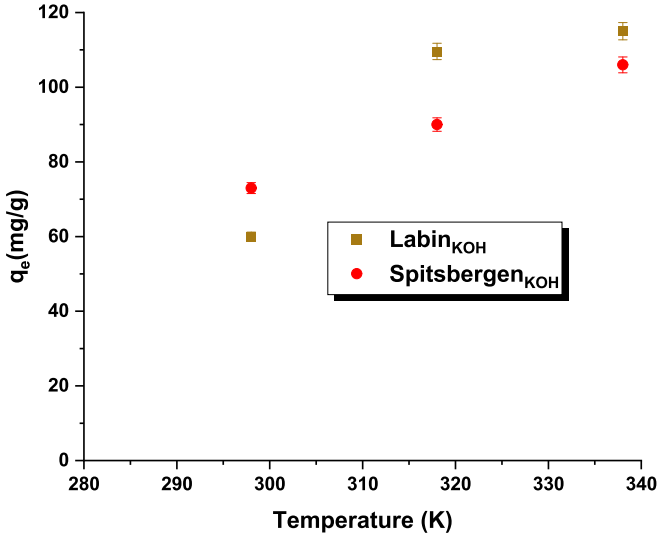

Fig. 8. Effect of temperature on the adsorption of Rhodamine B over Labin$_{KOH}$ and Spitsbergen$_{KOH}$.

Table 5
Thermodynamic parameters of Labin$_{KOH}$ and Spitsbergen$_{KOH}$.

Sample	Temperature (K)	ΔG^0 (kJ/mol)	ΔH^0 (kJ/mol)	ΔS^0 (J/mol × K)
Labin$_{KOH}$	298	−11.77	46.38	195.21
	318	−15.78		
	338	−19.58		
Spitsbergen$_{KOH}$	298	−5.86	35.58	139.93
	318	−9.51		
	338	−11.39		

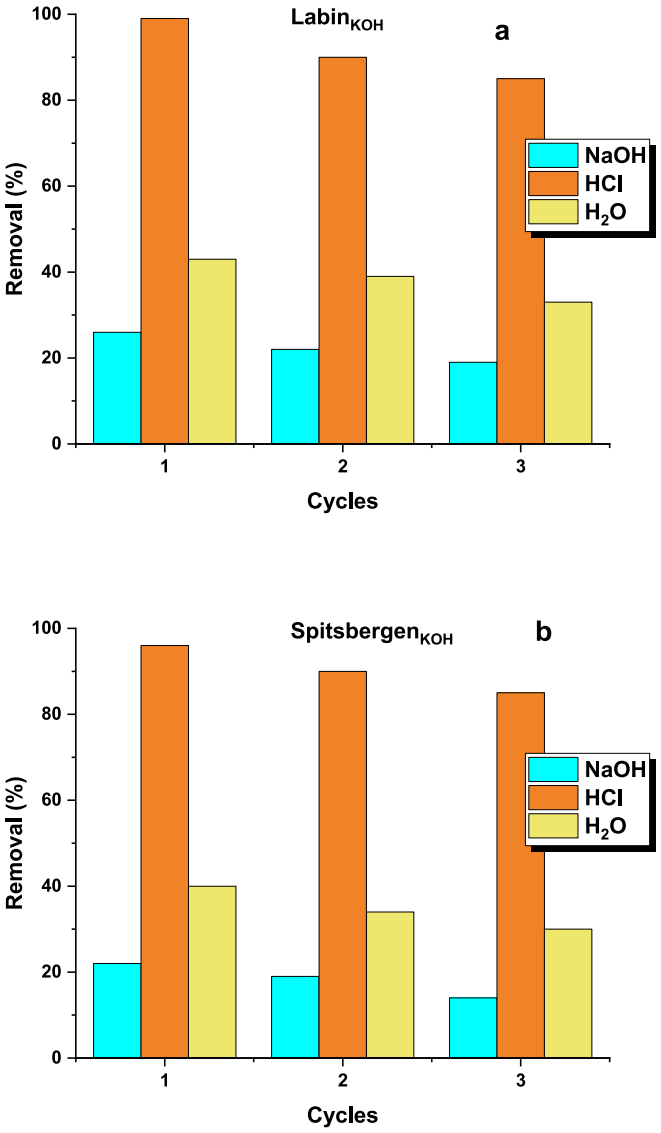

Fig. 9. Regeneration of Labin$_{KOH}$ (a) and Spitsbergen$_{KOH}$ (b) by different eluents.

activated carbons for organic compound removal. In the future, a combination of different eluents should be considered to enhance the efficiency of dye desorption.

In the final stage of the research, a comparison was made between the obtained results and the sorption capacities of carbon adsorbents described in the literature (Table 6). Additionally, a proposed mechanism for the adsorption of Rhodamine B on the obtained activated carbons was presented (Fig. 10). In general, the adsorbent's capacity for adsorption depends on the interactions between the adsorbate and the absorbent. Carbon materials may undergo π-π interactions, hydrophobic

Table 6
Comparison of adsorption performance of activated carbons over other adsorbents in literature.

Adsorbent	q_{max} (mg/g)	References
Labin$_{KOH}$	175	This study
Spitsbergen$_{KOH}$	82	This study
Activated carbon from bagasse pith	263.85	[29]
Biochar derived from tapioca peel	33.103	[30]
Cassava slag biochar	105.3	[31]
Activated carbon for white sugar	123.46	[32]
Activated biochar prepared from plaintain peels	84.41	[33]

interactions, hydrogen bonding and Lewis acid-base interactions with dyes, depending on their structure. The selected dye in this study contains various functional groups and aromatic rings. These functional groups are capable of forming π-π, hydrogen bonding, and electrostatic interactions with activated carbons. Additionally, π-π interactions are possible with dye samples and aromatic rings. Similar interactions have been noted and reported in literature [27,28]. The efficiency of the Labin$_{KOH}$ carbon in Rhodamine B removal was notably pronounced, exhibiting a substantial superiority over other adsorbents. Only the chemically activated carbon derived from *bagasse pith* using a 70 % orthophosphoric acid solution showed higher sorption capacity [29]. It is also worth noting that the second activated carbon produced in this study, Spitsbergen$_{KOH}$, demonstrated significantly higher sorption capacity compared to biochar derived from tapioca peel [30] and slightly lower capacity compared to activated carbon/biochar prepared from *Cassava slag* [31], white sugar [32], and plaintain peels [33].

4. Conclusion

In summary, activated carbons were obtained through the chemical activation of low-rank coals using potassium hydroxide. The physicochemical characterization showed that the synthesized adsorbents have moderately developed specific surface area and exhibit a mesoporous texture. The studies conducted revealed that the acid-base properties of activated carbons depend on the type of starting material used. The effectiveness of the activated carbons in removing Rhodamine B molecules from its aqueous solution was also investigated. The maximum adsorption capacity for Labin$_{KOH}$ carbon was 175 mg/g, and for Spitsbergen$_{KOH}$ carbon, it was 82 mg/g. The adsorption of Rhodamine B molecules on the surface of activated carbons followed the Langmuir model. Moreover, the adsorption equilibrium state for both carbons was reached within 240 min, which is highly favorable from an economic standpoint. The results of the kinetic studies demonstrated that there are chemical interactions between the adsorbent and the adsorbate since both activated carbons exhibited a correlation coefficient (R^2) of 0.999 for the pseudo-second order model. The results indicate that the adsorption of the studied dye on the surface of the samples increases with temperature, indicating an endothermic nature of the process, which is further confirmed by the values of ΔG^0 and ΔH^0 The most effective regenerative agent for the experiments turned out to be the 0.1 M HCl solution. Finally, the experiment showed that the most effective regenerative agent was the 0.1 M HCl solution.

The authors would like to thank Professor Izabela Nowak (Faculty of Chemistry, Adam Mickiewicz University, Poznań) for providing the research material.

CRediT authorship contribution statement

Aleksandra Bazan-Wozniak: Conceptualization, Methodology, Validation, Formal analysis, Investigation, Data curation, Visualization, Writing – original draft, Writing – review & editing. **Agnieszka Nosal-Wiercińska:** Validation, Resources, Writing – review & editing.

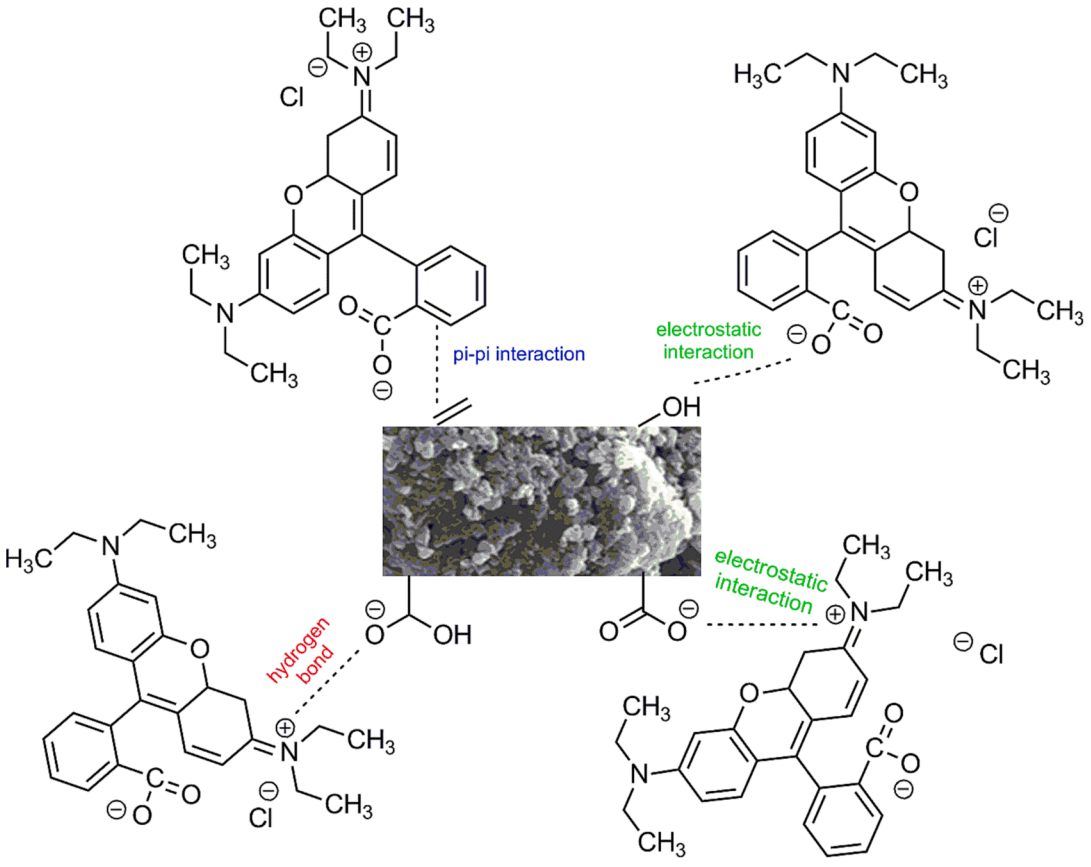

Fig. 10. The interaction mechanism between Rhodamine B and activated carbons.

Selehattin Yilmaz: Validation, Writing – review & editing. **Robert Pietrzak:** Conceptualization, Resources, Funding acquisition, Supervision, Writing – review & editing.

Declaration of Competing Interest

The authors declare that they have no known competing financial interests or personal relationships that could have appeared to influence the work reported in this paper.

Data availability

No data was used for the research described in the article.

References

[1] G. Song, W. Feng, Analysis of the spatial layout and influencing factors of pollution-intensive industries based on enterprise dynamics, Ecol. Ind. 152 (2023), 110378, https://doi.org/10.1016/j.ecolind.2023.110378.

[2] A. Javaid, M. Imran, S. Latif, N. Hussain, M. Bilal, Functionalized magnetic nanostructured composites and hybrids for photocatalytic elimination of pharmaceuticals and personal care products, Sci. Total Environ. 849 (2022), 157683, https://doi.org/10.1016/j.scitotenv.2022.157683.

[3] S. Some, R. Mondal, D. Mitra, D. Jain, D. Verma, S. Das, Microbial pollution of water with special reference to coliform bacteria and their nexus with environment, Energy Nexus. 1 (2021), 100008, https://doi.org/10.1016/j.nexus.2021.100008.

[4] R. Ma, R. Yuan, X. Fu, Climate change opportunity and corporate investment: Global evidence, J. Climate Finance. 3 (2023), 100013, https://doi.org/10.1016/j.jclimf.2023.100013.

[5] L. Thurakkal, M. Porel, Removal of cationic and anionic dyes from waste water in five seconds by a facile synthesis of a covalent organic polymer, Eur. Polym. J. 194 (2023), 112169, https://doi.org/10.1016/j.eurpolymj.2023.112169.

[6] S. Mallakpour, E. Azadi, M. Dinari, Removal of cationic and anionic dyes using Ca-alginate and Zn-Al layered double hydroxide/metal-organic framework, Carbohyd Polym. 301 (B) (2023), 120362, https://doi.org/10.1016/j.carbpol.2022.120362.

[7] A. Fouda, S.S. Salem, A.R. Wassel, M.F. Hamza, T.I. Shaheen, Optimization of green biosynthesized visible light active CuO/ZnO nano-photocatalysts for the degradation of organic methylene blue dye, Heliyon. 6 (9) (2020) e04896.

[8] H.A. Hamad, S.E. AbdElhafez, M.M. Elsenety, M.K. Sorour, N.K. Amin, O. Abdelwahab, E.-S.-Z. El-Ashtoukhy, Fabrication and characterization of functionalized lignin-based adsorbent prepared from black liquor in the paper industry for superior removal of toxic dye, Fuel 323 (2022), 124288, https://doi.org/10.1016/j.fuel.2022.124288.

[9] S. Wong, N. Ngadi, I.M. Inuwa, O. Hassan, Recent advances in applications of activated carbon from biowaste for wastewater treatment: A short review, J. Clean. Prod. 175 (2018) 361–375, https://doi.org/10.1016/j.jclepro.2017.12.059.

[10] Q. He, G. Wang, Z. Chen, Z. Miao, K. Wan, S. Huang, Adsorption of anionic azo dyes using lignite coke by one-step short-time pyrolysis, Fuel 267 (2020), 117140, https://doi.org/10.1016/j.fuel.2020.117140.

[11] Z. Liu, W. Shi, Y. Lei, Z. Xie, Novel polyamide/silica/chitosan covalent hybrid: One-step BIC/sol-gel preparation at room temperature and dual applications in Hg2+ electrochemical probing and dye adsorption, Carbohyd. Polym. 312 (2023), 120808, https://doi.org/10.1016/j.carbpol.2023.120808.

[12] J. Sharma, S. Sharma, U. Bhatt, V. Soni, Toxic effects of Rhodamine B on antioxidant system and photosynthesis of *Hydrilla verticillate*, JHM Letters. 3 (2022), 100069, https://doi.org/10.1016/j.hazl.2022.100069.

[13] J. Barros Goes e Silva, E. Rigoti, S. Pergher, Rhodamine B adsorption in ordered mesoporous materials: A comparison efficiency on KIT-6 and CMK-8, Results in Materials. 9 (2021) 100162. 10.1016/j.rinma.2020.100162.

[14] A. Bazan-Wozniak, R. Pietrzak, Adsorption of organic and inorganic pollutants on activated bio-carbons prepared by chemical activation of residues of supercritical extraction of raw plants, Chem. Eng. J. 393 (2020), 124785, https://doi.org/10.1016/j.cej.2020.124785.

[15] R. Mehdi, S.R. Naqvi, A.H. Khoja, R. Hussain, Biomass derived activated carbon by chemical surface modification as a source of clean energy for supercapacitor application, Fuel 348 (2023), 128529, https://doi.org/10.1016/j.fuel.2023.128529.

[16] A. Bazan-Wozniak, P. Nowicki, R. Pietrzak, Production of new activated bio-carbons by chemical activation of residue left after supercritical extraction of hops, Environ. Res. 161 (2018) 456–463, https://doi.org/10.1016/j.envres.2017.11.041.

[17] R. Davarnejad, S. Afshar, P. Etehadfar, Activated carbon blended with grape stalks powder: Properties modification and its application in a dye adsorption, Arab. J. Chem. 13 (5) (2020) 5463–5473, https://doi.org/10.1016/j.arabjc.2020.03.025.

[18] H. Wang, W. Wang, S. Zhou, X. Gao, Adsorption mechanism of Cr(VI) on woody-activated carbons, Heliyon. 9 (2) (2023) e13267.

[19] S. Ts, S.V. Khankhasaeva, M.V.U. Badmaeva, Adsorption of diclofenac onto Fe_2O_3-pillared montmorillonite: Equilibrium, kinetics and thermodynamic studies, J. Mol. Liq. 380 (2023), 121725, https://doi.org/10.1016/j.molliq.2023.121725.

[20] B. Krzyżyńska, A. Malaika, K. Ptaszyńska, A. Tolińska, P. Kirszensztejn, M. Kozłowski, Modified activated carbons for esterification of acetic acid with ethanol, Diam. Relat. Mater. 101 (2020), 107608, https://doi.org/10.1016/j.diamond.2019.107608.

[21] Y. Jiang, Q. Xie, Y. Zhang, C. Geng, B. Yu, J. Chi, Preparation of magnetically separable mesoporous activated carbons from brown coal with Fe_3O_4, Int. J. Min. Sci. Technol. 29 (3) (2019) 513–519, https://doi.org/10.1016/j.ijmst.2019.01.002.

[22] L.B. McCusker, F. Liebau, G. Engelhardt, Nomenclature of structural and compositional characteristics of ordered microporous and mesoporous materials with inorganic hosts (IUPAC Recommendations 2001), Pure Appl. Chem. 73 (2) (2001) 381–394, https://doi.org/10.1351/pac200173020381.

[23] F. Marrakchi, B.H. Hameed, E.H. Hummadi, Mesoporous biohybrid epichlorohydrin crosslinked chitosan/carbon–clay adsorbent for effective cationic and anionic dyes adsorption, Int. J. Biol. Macromol. 163 (2020) 1079–1086, https://doi.org/10.1016/j.ijbiomac.2020.07.032.

[24] A. Bazan-Wozniak, R. Pietrzak, Adsorption of cationic dye on nanostructured biocarbons: kinetic and thermodynamic study, Appl. Nanosci. (2023), https://doi.org/10.1007/s13204-023-02775-9.

[25] A. Bazan-Wozniak, S. Yilmaz, A. Nosal-Wiercińska, R. Pietrzak, Adsorption capacity of biocarbons from residue of supercritical extraction of raw plants, Pure Apply. Chem. 95 (2023) 545–561, https://doi.org/10.1515/pac-2023-0104.

[26] V. Watwe, S. Kulkarni, P. Kulkarni, Development of dried uncharred leaves of Ficus benjamina as a novel adsorbent for cationic dyes: Kinetics, isotherm, and batch optimization, Ind. Crop Prod. 195 (2023), 116449, https://doi.org/10.1016/j.indcrop.2023.116449.

[27] H. Zhao, X. Liu, Z. Cao, Y. Zhan, X. Shi, Y. Yang, J. Zhou, J. Xu, Adsorption behavior and mechanism of chloramphenicols, sulfonamides, and non-antibiotic pharmaceuticals on multi-walled carbon nanotubes, J. Hazard. Mater. 310 (2016) 235–245, https://doi.org/10.1016/j.jhazmat.2016.02.045.

[28] J. Xu, T. Sheng, Y. Hu, S.A. Baig, X. Lv, X. Xu, Adsorption–dechlorination of 2,4-dichlorophenol using two specified MWCNTs-stabilized Pd/Fe nanocomposites, Chem. Eng. J. 219 (2013) 162–173, https://doi.org/10.1016/j.cej.2013.01.010.

[29] H.M.H. Gad, A.A. El-Sayed, Activated carbon from agricultural by-products for the removal of Rhodamine-B from aqueous solution, J. Hazar. Mater. 168 (2–3) (2009) 1070–1081, https://doi.org/10.1016/j.jhazmat.2009.02.155.

[30] S. Vigneshwaran, P. Sirajudheen, P. Karthikeyan, S. Meenakshi, Fabrication of sulfur-doped biochar derived from tapioca peel waste with superior adsorption performance for the removal of Malachite green and Rhodamine B dyes, Sur. Interface. 23 (2021), 100920, https://doi.org/10.1016/j.surfin.2020.100920.

[31] J. Wu, J. Yang, G. Huang, C. Xu, B. Lin, Hydrothermal carbonization synthesis of cassava slag biochar with excellent adsorption performance for Rhodamine B, J. Clean. Prod. 251 (2020), 119717, https://doi.org/10.1016/j.jclepro.2019.119717.

[32] W. Xiao, Z.N. Garba, S. Sun, I. Lawan, L. Wang, M. Lin, Z. Yuan, Preparation and evaluation of an effective activated carbon from white sugar for the adsorption of rhodamine B dye, J. Clean. Prod. 253 (2020), 119989, https://doi.org/10.1016/j.jclepro.2020.119989.

[33] F.A. Adekola, S.B. Ayodele, A.A. Inyinbor, Activated biochar prepared from plaintain peels: Characterization and Rhodamine B adsorption data set, CDC. 19 (2019), 100170, https://doi.org/10.1016/j.cdc.2018.11.012.